Multidimensional wave propagation methods on moving grids

Sorin M. Mitran and Randall J. LeVeque
University of Washington, Department of Applied Mathematics, Box 352420,
Seattle, WA 98195-2420
E-mail: mitran, rjl@washington.edu

Version: November 28, 2001

The multidimensional wave propagation method [7] for solving hyperbolic partial differential equations is extended to moving grids of general geometry. Several examples are presented from acoustics, gas dynamics and elasticity. Some multiphysics examples, simultaneously solving different sets of conservation laws, are also included. The basic moving grid procedure is combined with adaptive mesh refinement to obtain an efficient algorithm capable of capturing phenomena with widely varying scales.

Key Words: Moving mesh methods, finite volume method, wave propagation, adaptive mesh refinement.

1. INTRODUCTION

Moving computational domains arise naturally in a number of applications described by hyperbolic evolution equations. Simulation of reciprocating, internal combustion engines involves the computation of the fluid flow in a cylinder with a moving piston wall [3]. The study of blood circulation leads to the problem of flow inside a domain with moving, flexible walls [10]. Acoustic [1] and electromagnetic radiation [12] from moving surfaces is of interest in a number of applications ranging from musical instruments [15] to micro-electro-mechanical systems (MEMS) [8]. In many applications the singularities that can arise in hyperbolic problems are of interest. The appearance of shocks in reciprocating engines significantly influences the engine's efficiency. Elastic waves in a solid medium may move fast enough that they induce singularities in an adjoining gas medium.

There is a considerable body of work on moving mesh methods applicable to such problems. We only cite a few entry points into the literature. Viecelly [14] treated the case of incompressible flow. Demirdzic and Peric [4] have presented a finite volume method with elements of arbitrary shape applicable to general flows. Thomas and Lombard [13] highlighted the importance of maintaining the same type of accuracy in the computation of geometric quantitites associated with grid motion as that used in the field variables. Subsequent work has confirmed this observation [9]. Recently Zwart, Raithby and Raw have presented a general finite volume method suitable for moving domains that exhibit large deformations [16].

In this paper we consider the problem of developing high-resolution finite volume methods to solve hyperbolic partial differential equations on moving grids in 2D and 3D. Such methods are known to be well suited for accurate capturing of singularities on stationary grids. High-resolution finite volume methods may be recast in wave propagation form [7] with certain advantages in achieving CFL numbers of unity and uniform treatment of both conservative and non-conservative hyperbolic problems. The wave propagation form has been applied to one-dimensional moving grids [6]. We are interested in extending the method to multi-dimensional moving grids so as to be able to treat some of the applications mentioned above. The point of view taken here is to use a time-dependent coordinate transformation from physical space to computational space. In physical space the grid is moving according to a motion which is imposed or perhaps influenced by the hyperbolic equation being solved. In computational space the grid is stationary. The essential difference is that in computational space the equation becomes more complicated, exhibiting space-time dependent coefficients even if such a dependence was not present in the equation expressed in physical space. As such, the problem is an important special case of the more general problem of hyperbolic equations with spatially dependent fluxes or coefficients.

The benefit of working in computational space is that Cartesian logical grid structure can be maintained. This is especially useful when the basic method is combined with adaptive mesh refinement (AMR) as is done in this work. The AMR framework adopted here is esentially that of Berger and LeVeque [2]. Previous work on combining adaptive meshing with moving grids includes [5]. The Cartesian grid structure makes is straightforward to carry out multi-physics computations in which different sets of conservation laws are solved on problem subdomains. The acoustic radiation from moving surfaces is presented as an example in this work, but the procedure may be readily extended to more complicated situations such as fluid-structure interactions [11].

2. PROBLEM FORMULATION

2.1. Time-dependent grid mappings

It is assumed that a non-singular transformation T from computational space to physical space may be defined at all times. We first consider the two-dimensional problem. All salient aspects of algorithm development are present in the 2D case. Extension to 3D is straightforward. The transformation between the computational space (ξ, η) and the physical space (x, y) is given by

$$T : \left\{ \begin{array}{l} x = X(\xi, \eta, t) \\ y = Y(\xi, \eta, t) \end{array} \right. . \tag{1}$$

The restriction of T to a given time t^n shall be denoted by T^n. The Jacobian of the transformation T shall be denoted by

$$J = \left| \begin{array}{cc} X_\xi & X_\eta \\ Y_\xi & Y_\eta \end{array} \right| = X_\xi Y_\eta - X_\eta Y_\xi \, . \tag{2}$$

Since T is assumed non-singular, we have $J \neq 0$.

2.2. Hyperbolic equations in conservation form

Consider the two-dimensional conservation equation governing the evolution in time of a field variable vector $q(x, y, t)$ with m components

$$q_t + f(q)_x + g(q)_y = \psi(x, y, t, q) \, . \tag{3}$$

The field variables and source term in computational space are

$$\tilde{q}(\xi,\eta,t) = q(X(\xi,\eta,t), Y(\xi,\eta,t), t),\ \ \tilde{\psi}(\xi,\eta,t,q) = \psi(X(\xi,\eta,t), Y(\xi,\eta,t), t, q)\,.$$

We also introduce the computational space fluxes $\tilde{f} = f(\tilde{q})$, $\tilde{g} = g(\tilde{q})$. The conservation equation in computational space is

$$(J\tilde{q})_t + F_\xi + G_\eta = J\tilde{\psi} \tag{4}$$

with the computational space fluxes

$$F^p = \begin{vmatrix} \tilde{f}^p & \tilde{g}^p \\ X_\eta & Y_\eta \end{vmatrix} - \begin{vmatrix} X_t & Y_t \\ X_\eta & Y_\eta \end{vmatrix} \tilde{q}^p \equiv \tilde{F}^p - U\tilde{q}^p, \tag{5}$$

$$G^p = \begin{vmatrix} X_\xi & Y_\xi \\ \tilde{f}^p & \tilde{g}^p \end{vmatrix} - \begin{vmatrix} X_\xi & Y_\xi \\ X_t & Y_t \end{vmatrix} \tilde{q}^p \equiv \tilde{G} - V\tilde{q}^p, \tag{6}$$

where $\tilde{q}^p$ is the p-th component of the vector q, with similar meanings for the flux components. Appendix A contains the derivation of these formulas. Note that the fluxes for the transformed equations contain a part that captures the physical fluxes expressed in the current curvilinear system, $\tilde{F}^p, \tilde{G}^p$ and a part that corresponds to flux due to grid motion, $U\tilde{q}^p, V\tilde{q}^p$. We shall call these the physical and grid motion fluxes in computational space, respectively. Whereas the initial flux functions $f(q)$, $g(q)$ depend only on the field variables, the grid transformation leads to physical fluxes in computational space that also exhibit coordinate dependence $\tilde{F}(\xi,\eta,t,\tilde{q})$, $\tilde{G}(\xi,\eta,t,\tilde{q})$.

Equation (4) can also be written in non-conservative form as

$$J\tilde{q}_t + \left(\tilde{\mathbf{F}}_{\tilde{q}} - U\mathbf{I}\right)\tilde{q}_\xi + \left(\tilde{\mathbf{G}}_{\tilde{q}} - V\mathbf{I}\right)\tilde{q}_\eta = J\tilde{\psi} - \left(J_t - U_\xi - V_\eta\right)\tilde{q}\,, \tag{7}$$

where $\mathbf{I}$ is the identity matrix and $\tilde{\mathbf{F}}_{\tilde{q}}$, $\tilde{\mathbf{G}}_{\tilde{q}}$ are the flux Jacobians in computational space

$$\tilde{\mathbf{F}}_{\tilde{q}} = Y_\eta \tilde{\mathbf{f}}_{\tilde{q}} - X_\eta \tilde{\mathbf{g}}_{\tilde{q}}, \quad \tilde{\mathbf{G}}_{\tilde{q}} = -Y_\xi \tilde{\mathbf{f}}_{\tilde{q}} + X_\xi \tilde{\mathbf{g}}_{\tilde{q}}$$

$$\tilde{\mathbf{f}}_{\tilde{q}} = \frac{\partial \tilde{f}}{\partial \tilde{q}}, \quad \tilde{\mathbf{g}}_{\tilde{q}} = \frac{\partial \tilde{g}}{\partial \tilde{q}}\,.$$

One can verify that

$$J_t - U_\xi - V_\eta = 0\,. \tag{8}$$

This is a statement of the change in infinitesimal area due to the grid motion. It is an instance of the geometric conservation law introduced by Thomas and Lombard [13]. The non-conservative form (7) shows that numerical errors in satisfying the geometric conservation law (8) act as a source term that may induce exponential growth in the field variables $\tilde{q}$.

2.3. Non-conservative hyperbolic equations

The non-conservative equation

$$q_t + \mathbf{A}(x,y)q_x + \mathbf{B}(x,y)q_y = \psi(x,y,t)$$

arises when studying wave propagation in non-uniform media among other applications. Introducing the coordinate mapping T leads to

$$\tilde{q}_t + (\mathbf{A} - X_t\mathbf{I})q_x + (\mathbf{B} - Y_t\mathbf{I})q_y = \psi$$

since $\tilde{q}_t = q_t + X_t q_x + Y_t q_y$. Expressing all derivatives in the computational space gives

$$\tilde{q}_t + \tilde{\mathbf{A}}\tilde{q}_\xi + \tilde{\mathbf{B}}\tilde{q}_\eta = \tilde{\psi}$$

with

$$\tilde{\mathbf{A}} = \frac{1}{J}\left[Y_\eta(\mathbf{A} - X_t\mathbf{I}) - X_\eta(\mathbf{B} - Y_t\mathbf{I})\right] = \frac{1}{J}\left[Y_\eta\mathbf{A} - X_\eta\mathbf{B} - U\mathbf{I}\right] ,$$

$$\tilde{\mathbf{B}} = \frac{1}{J}\left[X_\xi(\mathbf{B} - Y_t\mathbf{I}) - Y_\xi(\mathbf{A} - X_t\mathbf{I})\right] = \frac{1}{J}\left[X_\xi\mathbf{B} - Y_\xi\mathbf{A} - V\mathbf{I}\right] .$$

3. COMPUTATIONAL METHOD

3.1. Computational grid

A rectangular computational domain D is defined in which we use a uniform Cartesian grid with step sizes $\Delta\xi$, $\Delta\eta$. The grid lines are at $\xi_{i-1/2} = (i-1/2)\Delta\xi$, $\eta_{j-1/2} = (j-1/2)\Delta\eta$, $i = 1,\ldots,m_x, m_x+1$, $j = 1,\ldots,m_y, m_y+1$. A cell centered approach is adopted in which we define values $\tilde{Q}^n_{ij}$ to approximate $q(\xi,\eta,t^n)$ over the cell $\sigma_{ij} = [\xi_{i-1/2,j}, \xi_{i+1/2,j}] \times [\eta_{i,j-1/2}, \eta_{i,j+1/2}]$, $i = 1,2,\ldots,m_x$, $j = 1,2,\ldots,m_y$. The mapping T induces the grid node velocities $(\dot{x}_{i\pm1/2,j\pm1/2}(t), \dot{y}(t)_{i\pm1/2,j\pm1/2})$ in physical space. These velocities are assumed to be constant over a time step

$$(\dot{x}_{i\pm1/2,j\pm1/2}(t), \dot{y}_{i\pm1/2,j\pm1/2}(t)) = (\dot{x}^n_{i\pm1/2,j\pm1/2}, \dot{y}^n_{i\pm1/2,j\pm1/2}), \quad t \in [t^n, t^{n+1}] .$$

The grid velocities are assumed to vary linearly between nodes so that the cell edges trace out piecewise ruled surfaces in physical space.

3.2. Finite volume integration

To obtain a finite volume method, we integrate (4) over a rectangular cell in computational space σ_{ij} and over a time step $[t^n, t^{n+1}]$ to obtain

$$\begin{aligned}
&\iint_{\sigma_{ij}} \left[J(\xi,\eta,t^{n+1})\tilde{q}(\xi,\eta,t^{n+1}) - J(\xi,\eta,t^n)\tilde{q}(\xi,\eta,t^n)\right] d\xi\, d\eta \; + \\
&\int_{t^n}^{t^{n+1}} \int_{\eta_{j-1/2}}^{\eta_{j+1/2}} \left[F(\xi_{i+1/2},\eta,t) - F(\xi_{i-1/2},\eta,t)\right] d\eta\, dt \; - \\
&\int_{t^n}^{t^{n+1}} \int_{\xi_{i-1/2}}^{\xi_{i+1/2}} \left[G(\xi,\eta_{j+1/2},t) - G(\xi,\eta_{j-1/2},t)\right] d\xi\, dt = \Delta\xi\, \Delta\eta\, \Delta t\, \tilde{\Psi}^n_{ij}
\end{aligned} \tag{9}$$

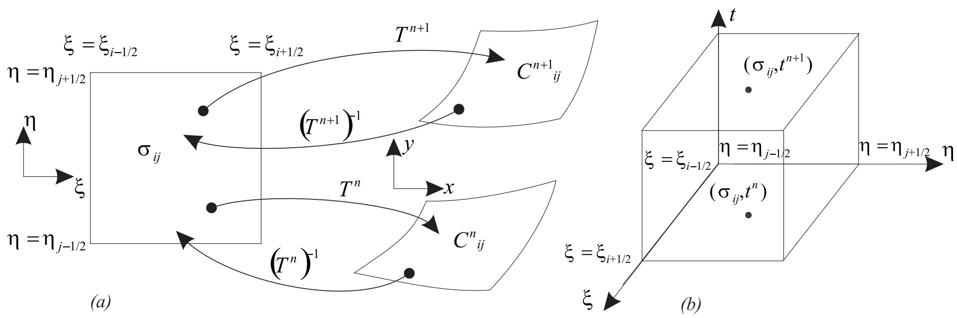

FIG. 1 (a) Transformation between computational and physical space. (b) Computational finite volume.

with

$$\tilde{\Psi}^n_{ij} = \frac{1}{\Delta\xi\,\Delta\eta\,\Delta t}\int_{t^n}^{t^{n+1}}\iint_{\sigma_{ij}}\tilde{\psi}(\xi,\eta,t)\,d\xi\,d\eta\,dt\,.$$

We can use the mean value theorem in computational space to obtain

$$\iint_{\sigma_{ij}} J(\xi,\eta,t^n)\tilde{q}(\xi,\eta,t^n)\,d\xi\,d\eta = J^n_{ij}\tilde{Q}^n_{ij}\Delta\xi\Delta\eta$$

where we use the notation $J^n_{ij} = J(\alpha_i,\beta_j,t^n)$, $\tilde{Q}^n_{ij} = \tilde{q}(\alpha_i,\beta_j,t^n)$ with $\alpha_i \in \left(\xi_{i-1/2},\xi_{i+1/2}\right)$ and $\beta_j \in \left(\eta_{j-1/2},\eta_{j+1/2}\right)$ being the points within the integration domain resulting from applying the mean value theorem. The mean value theorem can also be applied in physical space to give

$$\iint_{\sigma_{ij}} J(\xi,\eta,t^n)\tilde{q}(\xi,\eta,t^n)\,d\xi\,d\eta = \iint_{C^n_{ij}} q(x,y,t^n)\,dx\,dy = A^n_{ij}Q^n_{ij}$$

where C_{ij} is the image of the computational cell σ_{ij} through the transformation T and A_{ij} is the measure of C_{ij} (Fig. 1). We should have

$$A^n_{ij}Q^n_{ij} = \Delta\xi\Delta\eta J^n_{ij}\,\tilde{Q}^n_{ij}\,,$$

and this serves as a useful consistency condition on the specific numerical procedure used to evaluate the Jacobian.

Equation (9) leads to

$$\begin{gathered} J^{n+1}_{ij}\tilde{Q}^{n+1}_{ij} - J^n_{ij}\tilde{Q}^n_{ij} + \\ \frac{\Delta t}{\Delta\xi}\left(\mathcal{F}^n_{i+1/2,j} - \mathcal{F}^n_{i-1/2,j}\right) + \frac{\Delta t}{\Delta\eta}\left(\mathcal{G}^n_{i,j+1/2} - \mathcal{G}^n_{i,j-1/2}\right) = \tilde{\Psi}^n_{ij}, \end{gathered} \tag{10}$$

where $\mathcal{F},\mathcal{G}$ are the fluxes through the sides of the control volume over the time interval $[t^n,t^{n+1}]$.

3.3. Riemann problems in computational space

We can evaluate the fluxes $\mathcal{F},\mathcal{G}$ by solving Riemann problems along the directions ξ, η. Consider the ξ Riemann problem for $\psi = 0$. At the interface $\xi = \xi_{i-1/2}$

we assume that the left field variables have a constant value $\tilde{Q}^n_{i-1,j}$ over the cell $\sigma_{i-1,j}$. Similarily, to the right the value is $\tilde{Q}^n_{i,j}$ and constant over the cell $\sigma_{i,j}$. The η-derivative of $\tilde{q}$ is therefore null and from (7) we obtain

$$J\tilde{q}_t + \left(Y_\eta \tilde{\mathbf{f}}_{\tilde{q}} - X_\eta \tilde{\mathbf{g}}_{\tilde{q}} - U\mathbf{I}\right)\tilde{q}_\xi = 0,$$

This is a quasi-linear PDE with space-time varying coefficients. We obtain a linear PDE by introducing constant values of the physical flux Jacobians

$$\tilde{\mathbf{L}}_{i-1/2,j} = \left(\tilde{\mathbf{f}}_{\tilde{q}}\right)_{i-1/2,j}, \quad \tilde{\mathbf{M}}_{i-1/2,j} = \left(\tilde{\mathbf{g}}_{\tilde{q}}\right)_{i-1/2,j},$$

at the $\xi = \xi_{i-1/2}$ interface along the cell at $\eta_{j-1/2} \le \eta \le \eta_{j+1/2}$. These would typically depend on the field variables on the two sides of the interface

$$\tilde{\mathbf{L}}_{i-1/2,j} = \tilde{\mathbf{L}}_{i-1/2,j}(\tilde{Q}^n_{i-1,j}, \tilde{Q}^n_{i,j}), \quad \tilde{\mathbf{M}}_{i-1/2,j} = \tilde{\mathbf{M}}_{i-1/2,j}(\tilde{Q}^n_{i-1,j}, \tilde{Q}^n_{i,j}).$$

After making this approximation we obtain the equation

$$\tilde{q}_t + \frac{1}{J}\left(Y_\eta \tilde{\mathbf{L}}_{i-1/2,j} - X_\eta \tilde{\mathbf{M}}_{i-1/2,j} - U\mathbf{I}\right)\tilde{q}_\xi = 0. \tag{11}$$

Physical analysis of the behavior of the solution guides further approximation. Consider the two cells $C_{i-1,j}$, $C_{i,j}$ in physical space. In the cells we have constant field values $Q^n_{i-1,j}$, $Q^n_{i,j}$ at $t = t^n$. We expect the solution to the Riemann problem to be a family of waves $\mathcal{V}^p_{i-1/2,j}$ propagating with speeds that depend on the left and right states. Since these are assumed constant, the speeds shall be constant along the wave front. Each wave would propagate part of the initial discontinuity between $Q^n_{i-1,j}$ and $Q^n_{i,j}$. The wave fronts are line segments parallel to the initial orientation of the interface between $(x,y)^n_{i-1/2,j-1/2}$ and $(x,y)^n_{i-1/2,j+1/2}$ at $t = t^n$. Concurrently with the wave propagation, the interface traces out a ruled surface determined by the node velocities $(\dot{x},\dot{y})^n_{i-1/2,j\pm 1/2}$. The interface motion may be such that a particular wave $\mathcal{V}^1$ always remains to the left of the interface. Another wave $\mathcal{V}^3$ may always stay to the right of interface. Finally there is also the possibility that the interface intersects a wave front $\mathcal{V}^2$ for $t > t^n$. Fig. 2(a) depicts the various possibilities. In computational space, the wave fronts become ruled surfaces and the interface remains fixed. We again can have purely left going-waves $\mathcal{W}^1$, purely right-going wave $\mathcal{W}^3$ or mixed waves $\mathcal{W}^2$. Corresponding waves maintain their nature from physical space.

To obtain a stable, high-resolution method proper upwinding must be included. The possibility of mixed waves must be accounted for. Upon inspection of (11) we observe that the twisting of the wave front as η varies from $\eta_{i-1/2,j-1/2}$ to $\eta_{i-1/2,j+1/2}$ is given primarily by the the velocities X_t, Y_t contained in the U factor. We evaluate X_η, Y_η, J at a fixed point $\xi = \xi_{i-1/2}$, $\eta = \eta_j$, but maintain the η-dependence of the velocities X_t, Y_t. Equation (11) can be rewritten as

$$\tilde{q}_t + \left[\mathbf{P}_{i-1/2,j} - \omega_{i-1/2,j}(\eta)\mathbf{I}\right]\tilde{q}_\xi = 0,$$

$$\mathbf{P}_{i-1/2,j} = \left(\frac{Y_\eta}{J}\tilde{\mathbf{L}}\right)_{i-1/2,j} - \left(\frac{X_\eta}{J}\tilde{\mathbf{M}}\right)_{i-1/2,j},$$

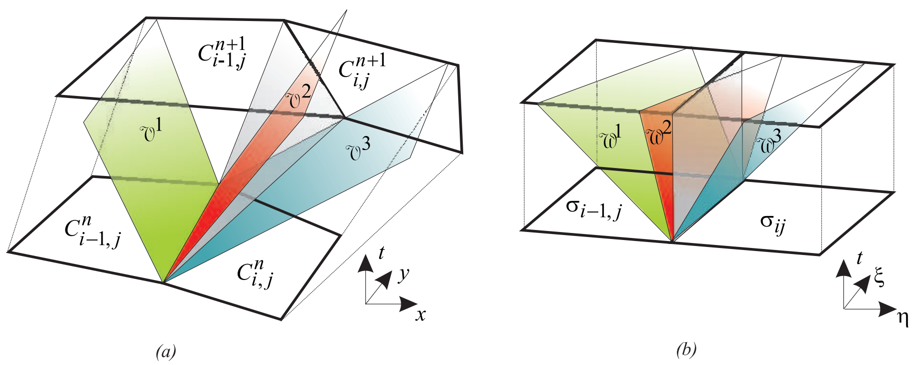

FIG. 2 (a) Waves ($\mathcal{V}^1$, $\mathcal{V}^2$, $\mathcal{V}^3$) and moving grid in physical space. The wavefronts are parallel to the initial orientation of the cell edge. $\mathcal{V}^1$ is a left-going wave, $\mathcal{V}^3$ is right-going. Due to the movement of the cell interface $\mathcal{V}^2$ has both a left-going and a right-going part. (b) Waves ($\mathcal{W}^1$, $\mathcal{W}^2$, $\mathcal{W}^3$) in computational space. The waves now trace out ruled surfaces. The nature of the waves remains the same, e.g. $\mathcal{W}^2$ is a mixed wave.

$$\omega_{i-1/2,j}(\eta) = \left(\frac{Y_\eta}{J}\right)_{i-1/2,j} X_t(\eta) - \left(\frac{X_\eta}{J}\right)_{i-1/2,j} Y_t(\eta)\,.$$

The dependence of the velocities upon η is given by linear interpolation between the node velocities, e.g.

$$X_t(\eta) = \frac{1}{\Delta\eta}\left[(\eta - \eta_{j-1/2})\,\dot{x}_{i-1/2,j+1/2} + (\eta_{j+1/2} - \eta)\,\dot{x}_{i-1/2,j-1/2}\right]$$

with a similar expression for $Y_t(\eta)$. We shall suppress the indices when their values can be ascertained from context to simplify the notation from now on.

Since the original problem is hyperbolic and the transformation T is nonsingular, the eigenvectors of $\mathbf{P}$ form a basis. Let $\mathbf{R}$ be the matrix of right eigenvectors of $\mathbf{P}$ and $\Lambda = \mathrm{diag}(\lambda^p)$ the diagonal matrix of eigenvalues of $\mathbf{P}$. Inserting the decomposition $\mathbf{P} = \mathbf{R}\Lambda\mathbf{R}^{-1}$ in (11) we obtain

$$\tilde{q}_t + \mathbf{R}\left[\Lambda - \omega(\eta)\mathbf{I}\right]\mathbf{R}^{-1}\tilde{q}_\xi = 0\,. \tag{12}$$

Since $\mathbf{R}$ does not depend on ξ or t we obtain the characteristic decomposition

$$\tilde{v}_t + \left[\Lambda - \omega(\eta)\mathbf{I}\right]\tilde{v}_\xi = 0\,, \tag{13}$$

with $\tilde{v} = \mathbf{R}^{-1}\tilde{q}$. Equation (13) is readily solved, so we have a solution to the Riemann problem in the approximation of frozen metric coefficients X_η, Y_η, J.

3.4. Wave propagation form

Since a solution to the Riemann problem is available one could use this to evaluate the fluxes $\mathcal{F}, \mathcal{G}$ needed in the update formula (10). Rather than doing this, we choose to recast the algorithm in terms of modifications to the finite volume averages brought about by the propagation of waves in computational space [7].

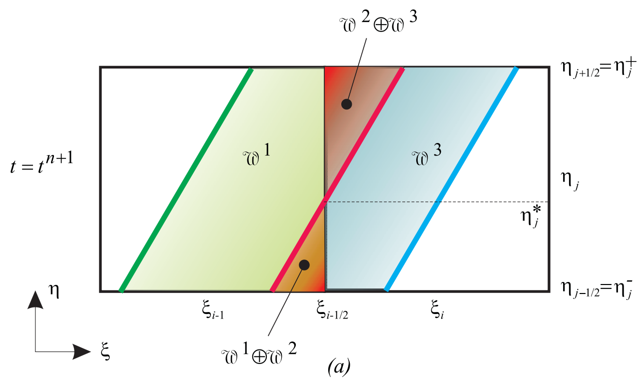

FIG. 3 (a) Areas of cells $\sigma_{i-1,j}$, σ_{ij} at $t = t^{n+1}$ affected by waves emanating from the jump in $\tilde{Q}$ at t^n. The left-going wave $\mathcal{W}^1$ affects the $\sigma_{i-1,j}$ cell average; the right-going wave $\mathcal{W}^3$ that of σ_{ij}. The mixed wave $\mathcal{W}^2$ updates both cells.

We now estimate what effect each wave has upon the cell average at the new time level $t = t^{n+1}$. First we split the initial jump among the eigenvectors of $\mathbf{P}$

$$\tilde{Q}^n_{i,j} - \tilde{Q}^n_{i-1,j} = \sum_{p=1}^{m_w} \alpha^p r^p_{i-1/2,j} \equiv \sum_{p=1}^{m_w} \mathcal{W}^p_{i-1/2,j} \, .$$

At $t = t^{n+1}$ a left-going or right-going wave will fill a trapezoid in cell $\sigma_{i-1,j}$, $\sigma_{i,j}$ respectively, see Fig. (3a). The new cell average is determined from

$$J^{n+1}_{ij} \tilde{Q}^{n+1}_{ij} = \frac{1}{\Delta\xi \Delta\eta} \iint_{\sigma_{ij}} J(\xi, \eta, t^{n+1}) \tilde{q}(\xi, \eta, t^{n+1}) \, d\xi \, d\eta \, .$$

The effect of any one wave $\mathcal{W}$ is change the The change in the cell average $\tilde{Q}^{n+1}_{i,j}$ brought about by the right-going wave $\mathcal{W}^3_{i-1/2,j}$ is

$$-\frac{\left[\lambda^3 - \omega(\eta_j)\right] \Delta t}{\Delta\xi} \mathcal{W}^3_{i-1/2,j} \, ,$$

corresponding to the area of the trapezoid filled by the $\mathcal{W}^3$ wave. A similar expression holds for the left-going wave. A mixed wave will fill two triangular portions in $\sigma_{i,j}$ and $\sigma_{i-1,j}$. Let η^*_j be the coordinate where $\lambda^2 - \omega(\eta^*_j) = 0$. The effect of the mixed wave $\mathcal{W}^2_{i,j}$ on the cell to the right $\sigma_{i,j}$ is

$$-\frac{\left[\lambda^2 - \omega(\eta^+_j)\right] \left|\eta^*_j - \eta^+_j\right| \Delta t}{2\Delta\xi\Delta\eta} \mathcal{W}^2_{i-1/2,j} \, ,$$

where η^+_j is the node where $\lambda^2 - \omega(\eta^*_j) > 0$, either $\eta^+ = \eta_{j-1/2}$ or $\eta^+ = \eta_{j+1/2}$. Similarily the effect of the mixed wave upon the cell to the left $\sigma_{i-1,j}$ is

$$-\frac{\left[\lambda^2 - \omega(\eta^-_j)\right] \left|\eta^*_j - \eta^-_j\right| \Delta t}{2\Delta\xi\Delta\eta} \mathcal{W}^2_{i-1/2,j} \, ,$$

with an analogous definition of η^-_j.

The first-order update (10) can be expressed in wave propagation form [7] as

$$\tilde{Q}_{ij}^{n+1} = \tilde{Q}_{ij}^{n} - \frac{\Delta t}{\Delta \xi}\left[\mathcal{A}^{+}\Delta\tilde{Q}_{i-1/2,j}^{n} + \mathcal{A}^{-}\Delta\tilde{Q}_{i+1/2,j}^{n}\right]$$

where $\mathcal{A}^{+}\Delta\tilde{Q}_{i-1/2,j}^{n}$ and $\mathcal{A}^{-}\Delta\tilde{Q}_{i+1/2,j}^{n}$ are the right-going and left-going fluctuations. We introduce the notation $\mu^{p}(\eta) = \lambda^{p} - \omega(\eta)$,

$$\left(\mu_{i-1/2,j}^{p}\right)^{+} = \begin{cases} \mu_{i-1/2,j}^{p}(\eta_j) & \text{if } \mu_{i-1/2,j\pm 1/2}^{p} > 0 \\ \dfrac{\left|\eta_j^{*} - \eta_j^{+}\right| \mu_{i-1/2,j\mp 1/2}^{p}}{2\Delta\eta} & \text{if } \mu_{i-1/2,j\mp 1/2}^{p} > 0,\ \mu_{i-1/2,j\pm 1/2}^{p} \le 0 \\ 0 & \text{if } \mu_{i-1/2,j1/2}^{p},\ \mu_{i-1/2,j+1/2}^{p} \le 0 \end{cases},$$

$$\left(\mu_{i-1/2,j}^{p}\right)^{-} = \begin{cases} \mu_{i-1/2,j}^{p}(\eta_j) & \text{if } \mu_{i-1/2,j-1/2}^{p},\ \mu_{i-1/2,j+1/2}^{p} < 0 \\ \dfrac{\left|\eta_j^{*} - \eta_j^{-}\right| \mu_{i-1/2,j\pm 1/2}^{p}}{2\Delta\eta} & \text{if } \mu_{i-1/2,j\mp 1/2}^{p} > 0,\ \mu_{i-1/2,j\pm 1/2}^{p} \le 0 \\ 0 & \text{if } \mu_{i-1/2,j-1/2}^{p},\ \mu_{i-1/2,j+1/2}^{p} \ge 0 \end{cases}.$$

The fluctuations may then be expressed as

$$\mathcal{A}^{+}\Delta\tilde{Q}_{i-1/2,j} = \sum_{p=1}^{m}\left(\mu_{i-1/2,j}^{p}\right)^{+}\mathcal{W}_{i-1/2,j}^{p},$$

$$\mathcal{A}^{-}\Delta\tilde{Q}_{i-1/2,j} = \sum_{p=1}^{m}\left(\mu_{i-1/2,j}^{p}\right)^{-}\mathcal{W}_{i-1/2,j}^{p}.$$

3.5. Conservative average flux Jacobians

We now turn to the problem of determining a suitable averages for the flux Jacobians. Consider just the ξ Riemann problem. We would like the scheme to be conservative and this leads to the condition

$$\mathbf{A}_{ij}\left(\tilde{Q}_{i+1,j}^{n+1} - \tilde{Q}_{i,j}^{n+1}\right) = F(\xi_i, \eta_j, t^{n+1}, \tilde{Q}_{i+1,j}^{n+1}) - F(\xi_i, \eta_j, t^{n+1}, \tilde{Q}_{i,j}^{n+1}).$$

Since $\mathbf{A}_{ij} = \tilde{\mathbf{A}}_{ij} - U_{ij}\mathbf{I}$ and $F_{ij} = \tilde{F}_{ij} - U_{ij}\tilde{Q}_{ij}$ we obtain

$$\tilde{\mathbf{A}}_{ij}\left(\tilde{Q}_{i+1,j}^{n+1} - \tilde{Q}_{i,j}^{n+1}\right) = \tilde{F}(\tilde{Q}_{i+1,j}^{n+1}) - \tilde{F}(\tilde{Q}_{i,j}^{n+1}).$$

Note that the space-time dependent part of the average flux Jacobian automatically satisfies the conservation condition. We are left just with the part that depends on the field variables.

3.6. Second order corrections

T

3.7. Transverse corrections

T

4. NON-CONSERVATIVE HYPERBOLIC EQUATIONS

T

5. THREE-DIMENSIONAL CASE

The procedures presented for the two-dimensional problem readily generalize to more dimensions. In three dimensions the general conservation law

$$q_t + f(q)_x + g(q)_y + h(q)_z = \psi(x, y, z, q, t) \tag{14}$$

becomes

$$(J\tilde{q})_t + F_\xi + G_\eta + H_\zeta = J\tilde{\psi} \tag{15}$$

with the computational space fluxes

$$\begin{aligned}
F &= \begin{vmatrix} \tilde{f} & \tilde{g} & \tilde{h} \\ X_\eta & Y_\eta & Z_\eta \\ X_\zeta & Y_\zeta & Z_\zeta \end{vmatrix} - \begin{vmatrix} X_t & Y_t & Z_t \\ X_\eta & Y_\eta & Z_\eta \\ X_\zeta & Y_\zeta & Z_\zeta \end{vmatrix} \tilde{q} \\
G &= \begin{vmatrix} X_\xi & Y_\xi & Z_\xi \\ \tilde{f} & \tilde{g} & \tilde{h} \\ X_\zeta & Y_\zeta & Z_\zeta \end{vmatrix} - \begin{vmatrix} X_\xi & Y_\xi & Z_\xi \\ X_t & Y_t & Z_t \\ X_\zeta & Y_\zeta & Z_\zeta \end{vmatrix} \tilde{q} \\
H &= \begin{vmatrix} X_\xi & Y_\xi & Z_\xi \\ X_\eta & Y_\eta & Z_\eta \\ \tilde{f} & \tilde{g} & \tilde{h} \end{vmatrix} - \begin{vmatrix} X_\xi & Y_\xi & Z_\xi \\ X_\eta & Y_\eta & Z_\eta \\ X_t & Y_t & Z_t \end{vmatrix} \tilde{q}
\end{aligned} \tag{16}$$

The flux Jacobian matrices are

$$\begin{aligned}
\frac{\partial F}{\partial \tilde{q}} &= (Y_\eta Z_\zeta - Y_\zeta Z_\eta) \frac{\partial f}{\partial \tilde{q}} + (Z_\eta X_\zeta - Z_\zeta X_\eta) \frac{\partial g}{\partial \tilde{q}} + (X_\eta Y_\zeta - X_\zeta Y_\eta) \frac{\partial h}{\partial \tilde{q}} \\
&\quad - [(Y_\eta Z_\zeta - Y_\zeta Z_\eta) X_t + (Z_\eta X_\zeta - Z_\zeta X_\eta) Y_t + (X_\eta Y_\zeta - X_\zeta Y_\eta) Z_t] I \\
\frac{\partial G}{\partial \tilde{q}} &= (Y_\zeta Z_\xi - Y_\xi Z_\zeta) \frac{\partial f}{\partial \tilde{q}} + (Z_\zeta X_\xi - Z_\xi X_\zeta) \frac{\partial g}{\partial \tilde{q}} + (X_\zeta Y_\xi - X_\xi Y_\zeta) \frac{\partial h}{\partial \tilde{q}} \\
&\quad - [(Y_\zeta Z_\xi - Y_\xi Z_\zeta) X_t + (Z_\zeta X_\xi - Z_\xi X_\zeta) Y_t + (X_\zeta Y_\xi - X_\xi Y_\zeta) Z_t] I \\
\frac{\partial H}{\partial \tilde{q}} &= (Y_\xi Z_\eta - Y_\eta Z_\xi) \frac{\partial f}{\partial \tilde{q}} + (Z_\xi X_\eta - Z_\eta X_\xi) \frac{\partial g}{\partial \tilde{q}} + (X_\xi Y_\eta - X_\eta Y_\xi) \frac{\partial h}{\partial \tilde{q}} \\
&\quad - [(Y_\xi Z_\eta - Y_\eta Z_\xi) X_t + (Z_\xi X_\eta - Z_\eta X_\xi) Y_t + (X_\xi Y_\eta - X_\eta Y_\xi) Z_t] I
\end{aligned} \tag{17}$$

These matrices have essentially the same structure as the flux Jacobian matrices in physical space.

6. ACCURACY

6.1. Advection

We first consider the advection problem

$$q_t + u\, q_x + v\, q_y = 0,$$

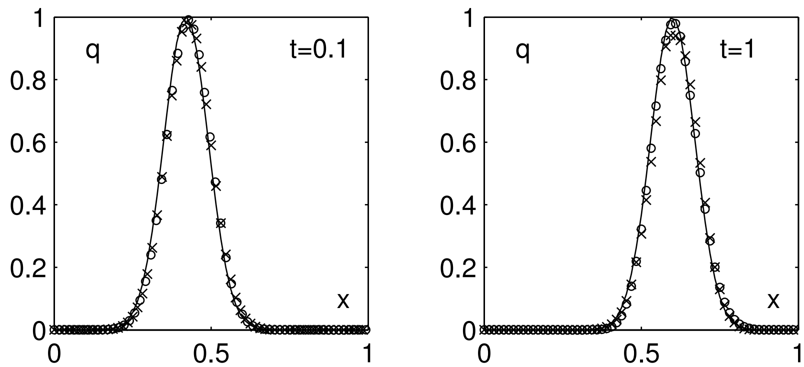

FIG. 4 Comparison of exact solution (line), fixed grid (x) and dilatational moving grid (o) computations for the advection problem.

$$q_0(x,y) = q(x,y,0) = \exp\left[-\left(\frac{x-x_c}{\delta_x}\right)^2 - \left(\frac{y-y_c}{\delta_y}\right)^2\right],$$

$(u,v) = (0.2, 0.1)$ to verify the over-all correctness of the method and to test accuracy. We shall compare the solution obtained numerically under various grid motions to the analytical solution $q(x,y,t) = q_0(x-ut, y-vt)$.

First we consider purely dilatational motions of the grid given by

$$X(\xi,\eta,t) = (1 + a_1 \sin\omega_1 t)\,\xi, \quad Y(\xi,\eta,t) = (1 + a_2 \sin\omega_2 t)\,\eta,$$

$$X_\xi = 1 + a_1 \sin\omega_1 t, \quad Y_\xi = X_\eta = 0, \quad Y_\eta = 1 + a_2 \sin\omega_2 t,$$

$$X_t = a_1\omega_1\xi\cos\omega_1 t, \quad Y_t = a_2\omega_2\eta\cos\omega_2 t.$$

Under such motions mixed waves cannot arise since the nodes on a cell edge have the same grid motion velocities. A one-dimensional slice through the data obtained from the computation on a fixed mesh, that obtained on the moving mesh and the analytical solution is shown in Fig. 4. The computations are carried out using second order corrections that eliminate the first order diffusive error proportional to $h\nabla^2 q$. The moving mesh result exhibits the same type of error as that computed on a fixed mesh, a slight displacement of the solution with respect to its exact position. As shown in [7], the moving mesh formulation is not formally second order since the system of equations becomes non-autonomous $(J\tilde{q})_t + F(\xi,\eta,t,\tilde{q})_\xi + G(\xi,\eta,t,\tilde{q})_\eta = 0$, even if the original equations in physical space was autonomous $q_t + f(q)_x + g(q)_y = 0$. We therefore expect an order of convergence intermediate between 1 and 2. This indeed is observed, as shown in Fig. 5.

A second test is carried out for purely rotational motions of the mesh given by

$$X(\xi,\eta,t) = \xi\cos\theta(t) + \eta\sin\theta(t), \quad Y(\xi,\eta,t) = -\xi\sin\theta(t) + \eta\cos\theta(t),$$

$$X_\xi = Y_\eta = \cos\theta(t), \quad X_\eta = \sin\theta(t), \quad Y_\xi = -\sin\theta(t),$$

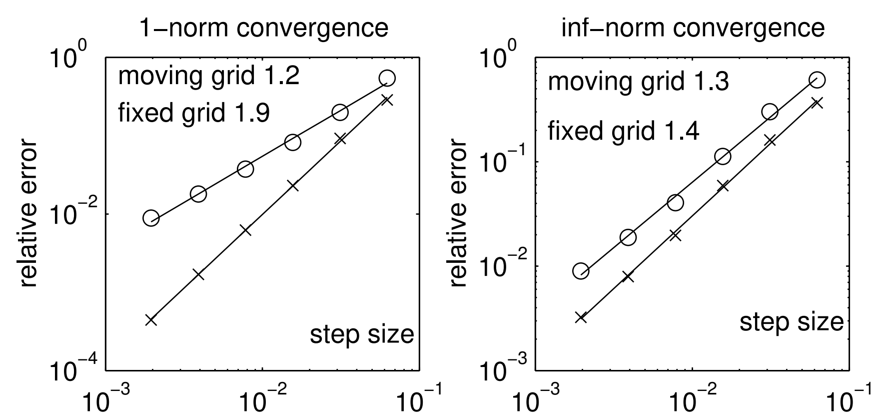

FIG. 5 Convergence plots of the fixed grid (x) and dilatational moving grid (o) computations for the advection problem at $t = 1$, after 250 steps have been executed.

$$X_t = Y\,\theta'(t), \quad Y_t = -X\,\theta'(t), \, \theta(t) = \theta_0 \sin \omega t.$$

The effect of grid shearing is investigated thorugh the mapping

$$X(\xi, \eta, t) = (\xi + a_1 \eta \sin \omega_1 t)\,, \quad Y(\xi, \eta, t) = (\eta + a_2 \xi \sin \omega_2 t)$$

7. APPLICATIONS

7.1.

7.2. Acoustics

7.3. Fluid dynamics

7.3.1. Euler equation eigensystem in computational space

The Riemann problems in computational space require the solutions to the eigenproblems

$$\frac{\partial F}{\partial \tilde{q}} r^F = \lambda^F r^F, \quad \frac{\partial G}{\partial \tilde{q}} r^G = \lambda^G r^G \tag{18}$$

The 2D Euler equations describing inviscid, compressible flow are

$$q_t + \vec{\nabla} \cdot \vec{\mathcal{F}} = 0, \quad \vec{\mathcal{F}} = f\,\vec{i} + g\,\vec{j}\,,$$

$$q = \left[\begin{array}{cccc} \rho & \rho u & \rho v & \rho E \end{array}\right]^T, \tag{19}$$

$$f = \left[\begin{array}{cccc} \rho u & \rho u^2 + p & \rho u v & \dfrac{uH}{\rho} \end{array}\right]^T, \, g = \left[\begin{array}{cccc} \rho v & \rho u v & \rho v^2 + p & \dfrac{vH}{\rho} \end{array}\right]^T$$

$$p = (\gamma - 1)(E - (u^2 + v^2)/2)\rho$$

Let $\vec{k} = k_x \vec{i} + k_y \vec{j}$, $k = (k_x^2 + k_y^2)^{1/2}$ represent an arbitrary direction. The right eigenvector matrix resulting from the eigenproblem $\left(\partial \vec{\mathcal{F}}/\partial q \cdot \vec{k}\right) r = \lambda r$ is

$$R(k_x, k_y) = \begin{pmatrix} 1 & 0 & 1 & 1 \\ u - ak_x/k & -k_y & u & u + ak_x/k \\ v - ak_y/k & k_x & v & v + ak_y/k \\ H - a\vec{k} \cdot \vec{V} & k_x v - k_y u & (u^2+v^2)/2 & H + a\vec{k} \cdot \vec{V} \end{pmatrix} \tag{20}$$

with $\vec{V} = u\,\vec{i} + v\,\vec{j}$, $H = a^2/(\gamma - 1) + (u^2 + v^2)/2$ and a the local sound velocity. The corresponding eigenvalues are

$$\lambda = (\vec{k} \cdot \vec{V} - ak, \vec{k} \cdot \vec{V}, \vec{k} \cdot \vec{V}, \vec{k} \cdot \vec{V} + ak). \tag{21}$$

We see that $R(Y_\eta, -X_\eta)$ is the right eigenvector matrix for $\partial F/\partial \tilde{q}$ and the eigenvalues are $\lambda_i^F = \lambda_i + X_\eta Y_t - X_t Y_\eta$, $i = 1, \ldots, 4$. Similarly $R(-Y_\xi, X_\xi)$ is the right eigenvector matrix for $\partial G/\partial \tilde{q}$ and the eigenvalues are $\lambda_i^G = \lambda_i + X_t Y_\xi - X_\xi Y_t$, $i = 1, \ldots, 4$.

7.3.2. Plane moving piston problem

We consider first the problem of a curved piston moving in a cylinder. The center of the piston is at

$$x_p(t) = b + l - r(1 - \cos\omega t) - \sqrt{l^2 - (r \sin\omega t)^2} \tag{22}$$

and the piston shape is assumed to be a circular arc of radius R, so the points (X_p, Y_p) on the piston surface are given by

$$X_p(\theta, t) = x_p(t) + R(\cos\theta - 1), \quad Y_p(\theta) = R \sin\theta\,. \tag{23}$$

The η coordinate lines intersect the piston at angles θ satisfying $R\sin\theta = (\eta - 1/2)d$. The range of θ is given by the limiting cases $R\sin\theta_{\min} = -d/2$, $R\sin\theta_{\max} = d/2$, The coordinate transformation between the computational space $D = [0,1] \times [0,1]$ and physical space is

$$x = X(\xi, \eta, t) = \xi X_p(\theta(\eta), t), \quad y = Y(\xi, \eta, t) = d(\eta - 1/2) \tag{24}$$

and we have the derivatives

$$X_\xi = X_p(t), \quad X_\eta = \frac{-\xi\,(\eta - 1/2)\,d^2}{\sqrt{R^2 - (\eta - 1/2)^2 d^2}}, \quad X_t = \xi \dot{x}_p(t) \tag{25}$$

$$Y_\xi = 0, \quad Y_\eta = d, \quad Y_t = 0$$

Axisymmetric moving piston problem
Consider now an axisymmetric piston

7.3.3. Three dimensional moving piston problem

A fully 3D piston is computed next

7.4. Coupled Elasticity and Acoustics

7.5. Coupled Elasticity and Fluid Dynamics

We now

7.5.1. *Plane stress eigensystem*

The equations describing a state of plane stress are

$$q_t + \vec{\nabla} \cdot \vec{\mathcal{F}} = 0, \quad \vec{\mathcal{F}} = f\,\vec{i} + g\,\vec{j}\,,$$

$$q = \begin{bmatrix} \varepsilon^{11} & \varepsilon^{12} & \varepsilon^{13} & U & V \end{bmatrix}^T,$$

$$f = \begin{bmatrix} U & V & 0 & a^2(\varepsilon^{11} + \nu\varepsilon^{22}) & b^2\varepsilon^{12} \end{bmatrix}^T$$

$$g = \begin{bmatrix} 0 & U & V & b^2\varepsilon^{12} & a^2(\nu\varepsilon^{11} + \varepsilon^{22}) \end{bmatrix}^T$$

$$a = c^2/(1-\nu^2), \quad b = c^2/(2(1+\nu)), \quad c^2 = E/\rho$$

with ε the strain tensor and (U, V) the displacement velocities

$$\varepsilon^{11} = u_x, \quad \varepsilon^{12} = u_y + v_x, \quad \varepsilon^{22} = v_y$$

$$U = u_t, \quad V = v_t \tag{26}$$

The right eigenvector matrix resulting from the eigenproblem $\left(\partial\vec{\mathcal{F}}/\partial q \cdot \vec{k}\right) r = \lambda r$ is

$$R(k_x, k_y) = \begin{pmatrix} k_y^2 - \nu k_x^2 & -\dfrac{k_x^2 c}{a} & \dfrac{k_x^2 c}{a} & \dfrac{k_x k_y c}{b} & -\dfrac{k_x k_y c}{b} \\ -2k_x k_y(1+\nu) & -2\dfrac{k_x k_y c}{a} & 2\dfrac{k_x k_y c}{a} & \dfrac{(k_y^2 - k_x^2)c}{b} & -\dfrac{(k_y^2 - k_x^2)c}{b} \\ k_x^2 - \nu k_y^2 & -\dfrac{k_y^2 c}{a} & \dfrac{k_y^2 c}{a} & -\dfrac{k_x k_y c}{b} & \dfrac{k_x k_y c}{b} \\ 0 & ck_x k & ck_x k & -ck_y & -ck_y \\ 0 & ck_y k & ck_y k & ck_x k & ck_x k \end{pmatrix}$$

The corresponding eigenvalues are

$$\lambda = \left(0, -\frac{ck}{\sqrt{2(1+\nu)}}, \frac{ck}{\sqrt{2(1+\nu)}}, -\frac{ck}{\sqrt{1-\nu^2}}, \frac{ck}{\sqrt{1-\nu^2}}\right). \tag{27}$$

8. CONCLUSIONS

APPENDIX A: CURVILINEAR COORDINATE CONSERVATION FORM

With F, G from (5,6) we have

$$F_\xi = Y_\eta \tilde{f}_\xi - (X_t Y_\eta)\tilde{q}_\xi - X_\eta \tilde{g}_\xi + X_\eta Y_t \tilde{q}_\xi \\ + Y_{\xi\eta}\tilde{f} - (X_t Y_\eta)_\xi\, \tilde{q} - X_{\xi\eta}\tilde{g} + (X_\eta Y_t)_\xi\, \tilde{q} \tag{28}$$

$$G_\eta = X_\xi \tilde{g}_\eta - (X_\xi Y_t)\tilde{q}_\eta - Y_\xi \tilde{f}_\eta + (X_t Y_\xi)\tilde{q}_\eta \\ + X_{\xi\eta}\tilde{g} - (X_\xi Y_t)_\eta \tilde{q} - Y_{\xi\eta}\tilde{f} + (X_t Y_\xi)_\eta \tilde{q} \tag{29}$$

Replacing these in the conservation equation (4) we have

$$J\tilde{q}_t + (Y_\eta \tilde{f}_\xi - Y_\xi \tilde{f}_\eta) + (X_\xi \tilde{g}_\eta - X_\eta \tilde{g}_\xi) + \tag{30}$$

$$(J_t - (X_t Y_\eta)_\xi + (X_\eta Y_t)_\xi - (X_\xi Y_t)_\eta + (X_t Y_\xi)_\eta)\, \tilde{q} = J\tilde{\psi}$$

Using (2) one can verify that the coefficient of $\tilde{q}$ in (30) is null, so equation (30) becomes

$$J\tilde{q}_t + Y_\eta \tilde{f}_\xi - Y_\xi \tilde{f}_\eta + X_\xi \tilde{g}_\eta - X_\eta \tilde{g}_\xi + (X_\eta Y_t - X_t Y_\eta)\tilde{q}_\xi + (X_t Y_\xi - X_\xi Y_t)\tilde{q}_\eta = J\tilde{\psi} \tag{31}$$

From $\tilde{q}(\xi, \eta, t) = q(X(\xi, \eta, t), Y(\xi, \eta, t), t)$ we have

$$\tilde{q}_t = q_x X_t + q_y Y_t + q_t\,,$$

$$\tilde{q}_\xi = q_x X_\xi + q_y Y_\xi\,,$$

$$\tilde{q}_\eta = q_x X_\eta + q_y Y_\eta\,, \tag{32}$$

and one can verify that

$$J\tilde{q}_t + (X_\eta Y_t - X_t Y_\eta)\tilde{q}_\xi + (X_t Y_\xi - X_\xi Y_t)\tilde{q}_\eta = J q_t\,, \tag{33}$$

so that (31) becomes

$$q_t + \frac{Y_\eta \tilde{f}_\xi - Y_\xi \tilde{f}_\eta}{J} + \frac{X_\xi \tilde{g}_\eta - X_\eta \tilde{g}_\xi}{J} = \tilde{\psi}\,. \tag{34}$$

By the implicit function theorem

$$\tilde{f}_x = \frac{Y_\eta \tilde{f}_\xi - Y_\xi \tilde{f}_\eta}{J}, \quad \tilde{g}_y = \frac{X_\xi \tilde{g}_\eta - X_\eta \tilde{g}_\xi}{J}, \tag{35}$$

so we obtain the initial conservation equation (3) noting that $\tilde{f} = f$, $\tilde{g} = g$, $\tilde{\psi} = \psi$ at corresponding points in the computational and physical domains.

The proof for the 3D case follows the same procedure.

ACKNOWLEDGMENTS

This work has been supported by grants NSF ... DOE ...

REFERENCES

[1] H. Antes and J. Baaran, *Noise radiation from moving surfaces*, Engineering Analysis with Boundary Elements, 25 (2001), pp. 725–740.

[2] M. Berger and R. LeVeque, *Adaptive mesh refinement using wave-propagation algorithms for hyperbolic systems*, SIAM J. Num. Analysis, 35 (1998), pp. 2298–2316.

[3] C. Cheng and H. K.S., *Numerical prediction of flow and thermal fields in a reciprocating piston-cylinder assembly*, Numerical Heat Transfer, A38 (2000), pp. 397–421.

[4] I. Demirdzic and M. Peric, *Finite volume method for prediction of fluid flow in arbitrarily shaped domains with moving boundaries*, Internat. J. Numer. Methods Fluids, 10 (1990), pp. 771–790.

[5] A. Egelja, M. Schafer, and F. Durst, *An adaptive grid eulerian method for the computation of free surface flows*, Int. J. Comp. Fl. Dyn., 10 (1998), pp. 213–224.

[6] R. Fazio and R. LeVeque, *Moving-mesh methods for one-dimensional hyperbolic problems using CLAWPACK*, Computers and Mathematics with Applications, (to appear).

[7] R. LeVeque, *Wave propagation algorithms for multidimensional hyperbolic systems*, J. Comp. Phys., 131 (1997), pp. 327–353.

[8] J. Moreland, A. Jander, J. Beall, P. Kabos, and S. Russek, *Micromechanical torque magnetometer for in situ thin-film measurements*, IEEE Trans. Magnetics, 37 (2001), pp. 2770–2772.

[9] S. Morton, R. Melville, and M. Visbal, *Accuracy and coupling issues of aeroelastic navier-stokes solutions on deforming meshes*, J. Aircraft, 35 (1998), pp. 798–805.

[10] M. Ralph and T. Pedley, *Flow in a channel with a moving indentation*, J. Fluid Mech., 190 (1988), pp. 87–112.

[11] M. Schäfer and I. Teschauer, *Numerical simulation of coupled fluid-solid problems*, Comput. Methods Appl. Mech. Engrg., 190 (2001), pp. 3645–3667.

[12] S. Shiryaeva, A. Grigor'ev, D. Belonozhko, and A. Golovanov, *Electromagnetic radiation of a nonlinearly oscillating charged drop*, Technical Phys. Lett., 27 (2001), pp. 875–877.

[13] P. Thomas and C. Lombard, *Geometric conservation law and its application to flow computations on moving grids*, AIAA Journal, 17 (1979), pp. 1030–1037.

[14] J. Viecelly, *A computing method for incompressible flows bounded by moving walls*, J. Comput. Phys., 8 (1979), pp. 119–143.

[15] L. Wang and C. Burroughs, *Acoustic radiation from bowed violins*, J. Acous. Soc. Am., 110 (2001), pp. 543–555.

[16] P. Zwart, G. Raithby, and M. Raw, *The integrated space-time finite volume method and its application to moving boundary problems*, J. Comp. Phys., 154 (1999), pp. 497–519.